

Global N-Body Simulation of Galactic Spiral Arms

Shugo Michikoshi¹  and Eiichiro Kokubo² 

¹ *Department for the Study of Contemporary Society, Kyoto Women's University, Imakumano, Higashiyama, Kyoto, 605-8501, Japan*

² *Division of Theoretical Astronomy, National Astronomical Observatory of Japan, Osawa, Mitaka, Tokyo 181-8588, Japan*

Accepted XXX. Received YYY; in original form ZZZ

ABSTRACT

The origin of galactic spiral arms is one of fundamental problems in astrophysics. Based on the local analysis Toomre (1981) proposed the swing amplification mechanism in which the self-gravity forms spiral arms as leading waves of stars rotate to trailing ones due to galactic shear. The structure of spiral arms is characterized by their number and pitch angle. We perform global N -body simulations of spiral galaxies to investigate the dependence of the spiral structure on disk parameters and compare the simulation results with the swing amplification model. We find that the spiral structure in the N -body simulations agrees well with that predicted by the swing amplification for the wide range of parameters. The pitch angle decreases with increasing the shear rate and is independent of the disk mass fraction. The number of spiral arms decreases with both increasing the shear rate and the disk mass fraction. If the disk mass fraction is fixed, the pitch angle increases with the number of spiral arms.

Key words: galaxies: spiral – methods: numerical

1 INTRODUCTION

The formation mechanism of galactic spiral arms in disk galaxies is one of important problems in galactic astronomy. The spiral arms are excited by tidal interactions with nearby companion galaxies (e.g., Oh et al. 2008; Dobbs et al. 2010) and by the central stellar bar (e.g., Buta et al. 2005). However, the spiral arms can also be excited and maintained without external perturbations. One theory to explain the origin of spiral arms in disk galaxies is swing amplification mechanism (Goldreich & Lynden-Bell 1965; Julian & Toomre 1966; Toomre 1981). During the rotation, a wave is amplified if Toomre's Q is 1-2. In N -body simulations of multi-arm spiral galaxies, it is observed that the spiral arms are transient and recurrent (e.g., Sellwood & Carlberg 1984; Sellwood 2000; Baba et al. 2009; Fujii et al. 2011). This feature can be understood by the swing amplification mechanism.

In a differentially rotating disk, if a perturber, such as a giant molecular cloud, exists, a stationary density structure around a perturber forms (Julian & Toomre 1966). Even without a explicit perturber, the density pattern can be amplified. If the leading wave exists, it rotates to a trailing wave due to the shear. If the self-gravity is sufficiently strong, the rotating wave is amplified during the rotation. These processes are called swing amplification (Goldreich & Lynden-Bell 1965; Julian & Toomre 1966; Toomre 1981). The ampli-

fied density patterns may correspond to spiral arms observed in the galaxies.

In the swing amplification theory, the local and linear approximations were adopted. First, the deviation of stellar orbits from the circular orbit on the disk midplane is assumed to be small compared to the orbital radius. This is local approximation or epicycle approximation (Binney & Tremaine 2008). In addition, the deviation of various quantities, such as the surface density, from the unperturbed state is assumed to be small, that is, the deviation from the circular orbit is small compared to the wavelength. Using this approximation, the hydrodynamic equation or Boltzmann equation in the local coordinate system is linearized (Goldreich & Lynden-Bell 1965; Julian & Toomre 1966). In this respect, this is linear approximation.

In the linear theory of swing amplification, a perturber or a seed leading wave is necessary for the growth of the spiral arms. D'Onghia et al. (2013) performed N -body simulations and examined the non-linear effect. Their simulations show that perturbers are not necessary once the spiral arms are developed. The spiral arm itself causes overdense and underdense regions that behave as perturbers and generate another spiral arm. This phenomenon cannot be explained only by the linear theory. Kumamoto & Noguchi (2016) clearly showed that the non-linear interaction between spiral arms forms overdense and underdense regions by the more controlled simulations.

However, we cannot still deny the importance of the linear theory of the swing amplification to explain the formation process of the spiral arm from a leading wave or a

* E-mail: michikos@kyoto-wu.ac.jp

† E-mail: kokubo@th.nao.ac.jp

perturber caused by the non-linear interaction. The linear theory of the swing amplification may explain some aspects of the basic physics of the spiral arm formation. In addition, the short-scale spiral structures in Saturn’s ring, so-called self-gravity wakes, are said to be formed by the swing amplification (Salo 1995; Michikoshi et al. 2015). The recent N -body simulation suggests that self-gravity wakes exists even in a ring around a small body (Michikoshi & Kokubo 2017). This type of structure may be ubiquitous. Therefore, it is important to understand physical mechanism of swing amplification.

In the series of our papers, we have investigated the swing amplification mechanism using the local linear theory and the local N -body simulations (Michikoshi & Kokubo 2014, 2016a,b). The global N -body simulations of the spiral arms show that the pitch angle of the spiral arms decreases with increasing the shear rate (Grand et al. 2013). This tendency is expected from the view of the swing amplification mechanism (Julian & Toomre 1966). From the local N -body simulations and the local linear analyses, we confirmed this trend and obtained the accurate pitch angle formula (Michikoshi & Kokubo 2014) (hereafter referred to as Paper I). The proposed pitch angle formula is consistent with other global N -body simulations (Grand et al. 2013; Baba 2015; Fujii et al. 2018). The physical understanding of the dependence of the pitch angle on the shear rate is given based on the phase synchronization of the epicycle motion (Michikoshi & Kokubo 2016b) (hereafter referred to as Paper III).

It is suggested that the number of spiral arms is inversely proportional to the disk mass fraction (Carlberg & Freedman 1985). D’Onghia et al. (2013) confirmed that the number of spiral arms is determined by the critical wavelength of the gravitational instability. It follows that the inverse relation between the disk mass and the number of spiral arm. D’Onghia (2015) adopted more detailed model of disk and halo models and obtained the number of spiral arms formula, which depends on the distance from the galactic center. Recently Fujii et al. (2018) performed global simulations that include a live bulge and dark matter halo. Their results show that a larger shear rate results in a smaller number of spirals. However, the dependence of the number of spiral arms on the shear rate has not been investigated quantitatively.

In the previous works, a factor X , which is the azimuthal wavelength normalized by the critical wavelength, is assumed to be 1–2. In general, X depends on the shear rate (Athanasoula 1984). Michikoshi & Kokubo (2016a) (hereafter referred to as Paper II) obtained the detailed formula of X , the pitch angle, the amplification factor, and the number of spiral arms as a function of disk parameters. It is suggested that X increases and the number of spiral arms decreases with increasing the shear rate. This prediction has not yet been confirmed by global simulations.

So far the results of the local N -body simulations agree well with the local linear analysis of the swing amplification mechanism (Paper I, II). However, in realistic spiral arms, the local approximation is not always valid. Especially, for the grand-design spiral arms, the local approximation would break down. Thus it is important to investigate the spiral structure by global N -body simulations.

In the present paper we extend local N -body simulations

to global ones and systematically investigate the dependencies of the number and pitch angle of spiral arms on the disk parameters. The outline of this paper is as follows. In Section 2, we introduce the model and simulation method. In Section 3, we give the results of the N -body simulations. In Section 4, we provide the intuitive explanation of the dependencies of the pitch angle and the number of spiral arms. We summarize our findings in Section 5.

2 METHOD

2.1 Model

In the many previous works, Hernquist profile or NFW profile as the dark halo model is often adopted (Hernquist 1990; Navarro et al. 1997). However, our aim is to examine the dependence on shear rate, disk mass fraction, and Q and to understand the physical mechanism of swing amplification. Thus, we introduce the somewhat artificial model for dark halo and disk to control these parameters directly, which is an straightforward extension of our local simulations presented in paper I, II. For the halo, we adopt the power-law model, which enables us to control the shear rate directly (e.g., Binney & Tremaine 2008). The similar dark halo model was also adopted in a recent controlled simulation (Kumamoto & Noguchi 2016). The density profile of the power-law density model follows

$$\rho_{\text{gh}} = \rho_{\text{h0}} \left(\frac{r}{r_0} \right)^{-\alpha}, \quad (1)$$

where r is the distance from the center, α is the power-law index of the density profile, r_0 is the typical scale length, and ρ_{h0} is the density at r_0 . Then, the corresponding orbital frequency is given as

$$\Omega_{\text{h}} = \Omega_0 \left(\frac{r}{r_0} \right)^{-\alpha/2}, \quad (2)$$

where Ω_0 is the orbital frequency at r_0 . The shear rate without the disk self-gravity is defined as

$$\Gamma_{\text{h}} = -\frac{d \log \Omega_{\text{h}}}{d \log r}. \quad (3)$$

If we neglect the disk self-gravity, the power-law density model gives the uniform shear rate $\Gamma_{\text{h}} = \alpha/2$. Observationally disk galaxies have the shear rate $0.4 \lesssim \Gamma_{\text{h}} \lesssim 1.5$ (Seigar et al. 2005).

The dark halo mass inside the sphere with radius r is $M_{\text{h}} = r^3 \Omega_{\text{h}}^2 / G$. From this, we can calculate the gravitational force from the dark halo at the point \mathbf{r} with $|\mathbf{r}| = r$, where the origin is the center of the galaxy. The gravitational acceleration by the halo is $\mathbf{a}_{\text{h}} = -\Omega_{\text{h}}^2 \mathbf{r}$, which diverges for $r \rightarrow 0$ when $\Gamma_{\text{h}} > 1/2$ ($\alpha > 1$). In addition, the circular velocity diverges when $\Gamma_{\text{h}} > 1$ ($\alpha > 2$). For avoiding the divergence, in calculating the acceleration, we introduce the softening parameter ϵ_{h} as $\mathbf{a}_{\text{h}} = -(GM_{\text{h}}/(r^2 + \epsilon_{\text{h}}^2)^{3/2})\mathbf{r}$. We adopt $\epsilon_{\text{h}} = 0.1r_0$. For $r \gg \epsilon_{\text{h}}$, this modification does not affect the result.

We introduce the mass scale

$$M_{\text{h0}} = \frac{r_0^3 \Omega_0^2}{G}. \quad (4)$$

We normalize the length, time, and mass by r_0 , Ω_0^{-1} , and

M_{h0} , respectively. In the following, the normalized quantities are denoted by a tilde on top.

The stellar disk surface density is given by an exponential model (e.g., Binney & Tremaine 2008)

$$\Sigma_d = \Sigma_{d0} e^{-\tilde{r}}, \quad (5)$$

where Σ_{d0} is the surface density at r_0 . The mass inside the sphere with radius r is

$$M_d(r) = M_{d,\infty} \left(1 - \frac{1 + \tilde{r}}{e^{\tilde{r}}}\right), \quad (6)$$

where $M_{d,\infty} = 2\pi\Sigma_{d0}r_0^2$ is the total mass of the stellar disk. In the following, we focus on the region with $1 < \tilde{r} < 2$. We define the disk mass fraction f as

$$f = \frac{M_d(2r_0)}{M_d(2r_0) + M_h(2r_0)}. \quad (7)$$

It is often assumed that the ratio of the radial velocity dispersion to the surface density is constant (Lewis & Freeman 1989; Hernquist 1993). Then, Q depends on the distance from the galactic center. However, the aim of this paper is to elucidate the dependence on the disk parameters. Thus, we assume that the initial Toomre's Q , Q_{ini} , of the disk is uniform. From this, we calculate the initial radial velocity dispersion σ_r . The initial azimuthal velocity dispersion σ_θ is $\sigma_\theta/\sigma_r = \kappa/2\Omega_h$. Here we assume that the initial vertical velocity dispersion σ_z is given by an equilibrium ratio, which is $\sigma_z/\sigma_r = 0.3\kappa/\Omega_h + 0.2$, where κ is the epicycle frequency for simplicity (e.g., Ida et al. 1993, Paper I). Using the epicycle approximation, we determine the initial velocity of each particle with the random phase of the epicycle motion. Since the generated disk is not exactly in an equilibrium, the artificial axisymmetric structure appears first. To remove this structure, we let the disk evolve for $\tilde{t}/2\pi = 15$ under the constraint of the rotational symmetry of the surface density by randomizing the azimuthal positions of particles (McMillan & Dehnen 2007; Fujii et al. 2011). Then we adopt it as the initial disk.

The number of stars is $N = 3 \times 10^6$. We introduce the softening length of the self-gravity between stars ϵ . We adopt $\tilde{\epsilon} = 0.01$, which is sufficiently small to resolve the structures. In the models where the small scale structures appear ($f = 0.05$ and 0.1) we also perform simulations with $\tilde{\epsilon} = 0.005$ and confirm that the following results do not change. In the following we vary f , Q_{ini} , and Γ_h . The disk parameters are listed in Table 1. The models with $\Gamma_h = 1$ (models 7, 9 and 13–30) correspond to disks with flat rotation curve. The circular velocity and shear rate of model 7 are shown in Fig. 1. The actual shear rate Γ can deviate from Γ_h slightly due to the disk self-gravity and the velocity dispersion. From the averaged rotational velocity in the simulations, we calculate Γ , which is summarized in Table 1. The difference between Γ and Γ_h is small. If f is not so large, we can neglect the disk contribution to the rotational velocity, which means $\Omega \simeq \Omega_h$ where Ω is the orbital frequency. Then the actual shear rate is approximated by Γ_h .

We use the simulation code based on FDPS, which is a general-purpose, high-performance library for particle simulations (Iwasawa et al. 2016) with the Phantom-GRAPE module (Tanikawa et al. 2012, 2013). We adopt a leapfrog integrator with the fixed timestep $\Delta\tilde{t} = 2\pi/1000$.

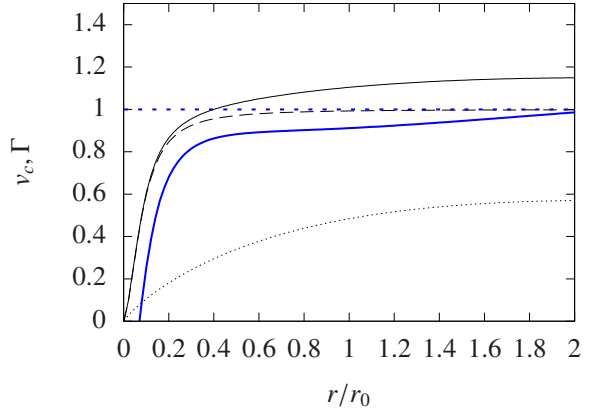


Figure 1. Circular velocity v_c and shear rate Γ of model 7. The thin solid curve shows the circular velocity. The thin dashed and dotted curves show the circular velocity contributed by the halo and disk, respectively. The thick solid curve shows the shear rate calculated from the circular velocity. The thick dotted line shows Γ_h .

2.2 Analysis of Spiral Arms

In order to analyze the spiral arms quantitatively, we calculate their number and pitch angle using the Fourier coefficients. As stated in Section 2.1, we focus on the disk region of $1.0 < \tilde{r} < 2.0$ where the softening effect of the acceleration from the halo is negligible. We divide the region into 10 annuli with width $\Delta\tilde{r} = 0.1$. In each annulus, we calculate the surface density $\Sigma(\tilde{r}, \phi, \tilde{t})$, where ϕ is the azimuthal angle. The Fourier coefficient at radius \tilde{r} for $m \geq 1$ is defined by

$$A_m(\tilde{r}, \tilde{t}) = \frac{1}{\pi} \int_0^{2\pi} \frac{\Sigma(\tilde{r}, \phi, \tilde{t})}{\bar{\Sigma}(\tilde{r}, \tilde{t})} \exp(-im\phi) d\phi, \quad (8)$$

where $\bar{\Sigma}(\tilde{r}, \tilde{t})$ is the azimuthally averaged surface density,

$$\bar{\Sigma}(\tilde{r}, \tilde{t}) = \frac{1}{2\pi} \int_0^{2\pi} \Sigma(\tilde{r}, \phi, \tilde{t}) d\phi. \quad (9)$$

For $m = 0$, the Fourier coefficient is $A_0 = 1$. Conversely, we can reconstruct the surface density from $A_m(\tilde{r}, \tilde{t})$

$$\frac{\Sigma(\tilde{r}, \phi, \tilde{t})}{\bar{\Sigma}(\tilde{r}, \tilde{t})} = \sum_{m=0}^{\infty} |A_m(\tilde{r}, \tilde{t})| \cos(m\phi + \phi_m), \quad (10)$$

where $\phi_m = \tan^{-1}(\Im(A_m(\tilde{r}, \tilde{t}))/\Re(A_m(\tilde{r}, \tilde{t})))$ is the shape function.

We estimate the number of spiral arms using Fourier coefficient. First we find $m_{\max}(\tilde{r}, \tilde{t})$ that has the maximum amplitude $|A_m(\tilde{r}, \tilde{t})|$ of the annulus with radius \tilde{r} at \tilde{t} . Since the number of spiral arms varies with the radius (Fujii et al. 2011), $m_{\max}(\tilde{r}, \tilde{t})$ has the relatively large dispersion. Thus, we calculate the mean value of $m_{\max}(\tilde{r}, \tilde{t})$ at each \tilde{t} , $m_{\text{mean}}(\tilde{t}) = \langle m_{\max}(\tilde{r}, \tilde{t}) \rangle_{\tilde{r}}$, where $\langle X \rangle_Y$ denotes the average of X with respect to the variable Y . In calculating average, we adopt the interquartile mean for avoiding the influence from outliers. Fig. 2 shows the time evolution of $m_{\text{mean}}(\tilde{t})$. For $\Gamma_h = 0.5$, $m_{\text{mean}}(\tilde{t})$ is almost constant throughout the simulation, which is about $\simeq 9$. On the other hand, for $\Gamma_h = 1.0$ and 1.5 , $m_{\text{mean}}(\tilde{t})$ decreases with time until $\tilde{t}/2\pi \simeq 10$ and

Table 1. Disk Parameters and Results

Model	f	Q_{ini}	Γ_{h}	Γ	Q_{mean}	\bar{m}	$\bar{\theta}$
1	0.20	1.2	0.4	0.48 ± 0.03	1.23 ± 0.05	10.2 ± 2.5	39.2 ± 27.1
2	0.20	1.2	0.5	0.57 ± 0.03	1.27 ± 0.07	9.2 ± 2.0	36.1 ± 13.2
3	0.20	1.2	0.6	0.65 ± 0.03	1.31 ± 0.08	8.1 ± 1.0	32.9 ± 10.1
4	0.20	1.2	0.7	0.73 ± 0.03	1.37 ± 0.10	6.8 ± 1.0	29.9 ± 9.2
5	0.20	1.2	0.8	0.81 ± 0.03	1.42 ± 0.10	6.1 ± 1.0	28.0 ± 8.1
6	0.20	1.2	0.9	0.90 ± 0.03	1.46 ± 0.11	5.4 ± 1.5	25.7 ± 7.9
7	0.20	1.2	1.0	0.98 ± 0.03	1.48 ± 0.10	4.8 ± 1.0	24.0 ± 7.2
8	0.20	1.2	1.1	1.06 ± 0.03	1.48 ± 0.11	4.0 ± 1.0	20.7 ± 8.2
9	0.20	1.2	1.2	1.14 ± 0.02	1.43 ± 0.09	3.6 ± 1.0	19.6 ± 6.1
10	0.20	1.2	1.3	1.23 ± 0.02	1.42 ± 0.10	3.2 ± 0.5	16.9 ± 6.0
11	0.20	1.2	1.4	1.31 ± 0.01	1.41 ± 0.08	2.5 ± 0.5	15.6 ± 6.2
12	0.20	1.2	1.5	1.41 ± 0.01	1.48 ± 0.06	2.3 ± 0.5	13.3 ± 4.5
13	0.40	1.2	0.4	0.53 ± 0.07	1.32 ± 0.14	4.6 ± 1.0	32.4 ± 12.5
14	0.40	1.2	0.5	0.60 ± 0.07	1.36 ± 0.13	3.8 ± 0.5	31.0 ± 8.3
15	0.40	1.2	0.6	0.67 ± 0.06	1.41 ± 0.15	4.4 ± 1.0	34.2 ± 10.5
16	0.40	1.2	0.7	0.74 ± 0.06	1.44 ± 0.14	3.5 ± 0.5	25.6 ± 15.8
17	0.40	1.2	0.8	0.80 ± 0.06	1.45 ± 0.15	3.5 ± 0.5	27.2 ± 11.9
18	0.40	1.2	0.9	0.87 ± 0.05	1.44 ± 0.13	3.2 ± 0.5	25.4 ± 9.6
19	0.40	1.2	1.0	0.94 ± 0.04	1.43 ± 0.11	2.8 ± 0.5	22.5 ± 9.1
20	0.40	1.2	1.1	1.02 ± 0.03	1.38 ± 0.07	2.4 ± 0.5	20.4 ± 10.6
21	0.40	1.2	1.2	1.10 ± 0.03	1.40 ± 0.07	2.4 ± 0.5	18.0 ± 6.7
22	0.40	1.2	1.3	1.18 ± 0.02	1.40 ± 0.06	2.0 ± 0.0	15.5 ± 6.2
23	0.40	1.2	1.4	1.27 ± 0.03	1.49 ± 0.09	2.0 ± 0.0	14.5 ± 5.9
24	0.40	1.2	1.5	1.38 ± 0.04	1.75 ± 0.14	2.0 ± 0.0	13.8 ± 10.3
25	0.05	1.2	1.0	0.99 ± 0.01	1.71 ± 0.07	14.5 ± 3.0	-14.3 ± 35.4
26	0.10	1.2	1.0	0.99 ± 0.02	1.59 ± 0.08	8.0 ± 1.0	23.0 ± 15.5
27	0.15	1.2	1.0	0.98 ± 0.02	1.52 ± 0.10	6.1 ± 1.0	24.5 ± 7.2
28	0.20	1.2	1.0	0.98 ± 0.03	1.48 ± 0.10	4.8 ± 1.0	24.0 ± 7.2
29	0.25	1.2	1.0	0.97 ± 0.04	1.45 ± 0.11	4.0 ± 1.0	22.6 ± 8.3
30	0.30	1.2	1.0	0.96 ± 0.04	1.45 ± 0.13	3.5 ± 0.5	23.9 ± 8.5
31	0.35	1.2	1.0	0.96 ± 0.04	1.42 ± 0.12	3.4 ± 0.5	23.5 ± 7.6
32	0.40	1.2	1.0	0.94 ± 0.04	1.43 ± 0.11	2.8 ± 0.5	22.5 ± 9.1
33	0.20	1.0	1.0	0.98 ± 0.04	1.78 ± 0.12	4.0 ± 1.0	25.4 ± 9.2
34	0.20	1.1	1.0	0.98 ± 0.03	1.58 ± 0.12	4.6 ± 0.5	24.0 ± 8.6
35	0.20	1.2	1.0	0.98 ± 0.03	1.48 ± 0.10	4.8 ± 1.0	24.0 ± 7.2
36	0.20	1.3	1.0	0.98 ± 0.02	1.44 ± 0.06	5.0 ± 1.0	23.9 ± 7.5
37	0.20	1.4	1.0	0.97 ± 0.02	1.47 ± 0.03	4.5 ± 0.5	22.6 ± 9.1
38	0.20	1.5	1.0	0.97 ± 0.02	1.55 ± 0.02	4.4 ± 0.5	21.5 ± 9.5
39	0.20	1.6	1.0	0.97 ± 0.01	1.63 ± 0.03	4.4 ± 0.5	21.2 ± 16.7
40	0.20	1.7	1.0	0.97 ± 0.01	1.73 ± 0.03	5.2 ± 1.5	19.9 ± 19.3
41	0.20	1.8	1.0	0.97 ± 0.01	1.82 ± 0.04	5.1 ± 2.5	16.9 ± 19.4
42	0.20	1.9	1.0	0.97 ± 0.01	1.92 ± 0.04	8.7 ± 12.0	13.8 ± 34.3

then becomes almost constant. Thus we calculate the number of spiral arms by the time average over $10 < \tilde{t}/2\pi < 20$, $\bar{m} = \langle m_{\text{max}}(\tilde{r}, \tilde{t}) \rangle_{\tilde{r}, \tilde{t}}$.

The pitch angle θ_m for mode m is defined by the shape function (e.g., Binney & Tremaine 2008),

$$\cot \theta_m(\tilde{r}, \tilde{t}) = \frac{\tilde{r}}{m} \frac{d\phi_m}{d\tilde{r}} \simeq \frac{\tilde{r}}{2m\Delta\tilde{r}} (\phi_m(\tilde{r} + \Delta\tilde{r}, \tilde{t}) - \phi_m(\tilde{r} - \Delta\tilde{r}, \tilde{t})). \quad (11)$$

We calculate $\theta_{\text{max}}(\tilde{r}, \tilde{t})$ of the dominant mode with $m_{\text{max}}(\tilde{r}, \tilde{t})$. We calculate $\theta_{\text{mean}}(\tilde{t}) = \langle \theta_{\text{max}}(\tilde{r}, \tilde{t}) \rangle_{\tilde{r}}$ by averaging $\theta_{\text{max}}(\tilde{r}, \tilde{t})$ over \tilde{r} . Fig. 2 shows the time evolution of $\theta_{\text{mean}}(\tilde{t})$. Although the pitch angle has the large dispersion, there seems no clear trend. Finally we obtain the time average of the pitch angle over $10 < \tilde{t}/2\pi < 20$, $\bar{\theta} = \langle \theta_{\text{max}}(\tilde{r}, \tilde{t}) \rangle_{\tilde{r}, \tilde{t}}$.

Fig. 3 demonstrates the estimated spiral arms for the surface density distribution at $\tilde{t}/2\pi = 15$ for model 7 where $\Gamma_{\text{h}} = 1.0$, $f = 0.2$, and $Q_{\text{ini}} = 1.2$. Their estimated number and pitch angle are $\bar{m} = 4.8$ and $\bar{\theta} = 24.0^\circ$, which are consistent

with the numerical results. Assuming $m = 5$ and $\theta = 24.0^\circ$, we draw the logarithmic spiral. The j -th logarithmic spiral ($j = 0, 1, 2, \dots, m-1$) is given by

$$\phi = -\frac{\phi_m(r_0)}{m} - \frac{1}{\tan \theta} \log \left(\frac{r}{r_0} \right) + \frac{2\pi j}{m}, \quad (12)$$

where $\phi_m(r_0)$ is the phase at radius r_0 . We find that the logarithmic spiral arms with the estimated spiral parameters agree with the simulation. This indicates that the dependence of the pitch angle on the galactocentric distance is weak.

3 RESULTS

3.1 Spiral Arm Structures

Fig. 4 shows the spiral arm structures for $\Gamma_{\text{h}} = 0.5$ (model 2), $\Gamma_{\text{h}} = 1.0$ (model 7), and $\Gamma_{\text{h}} = 1.5$ (model 12) where $f = 0.2$.

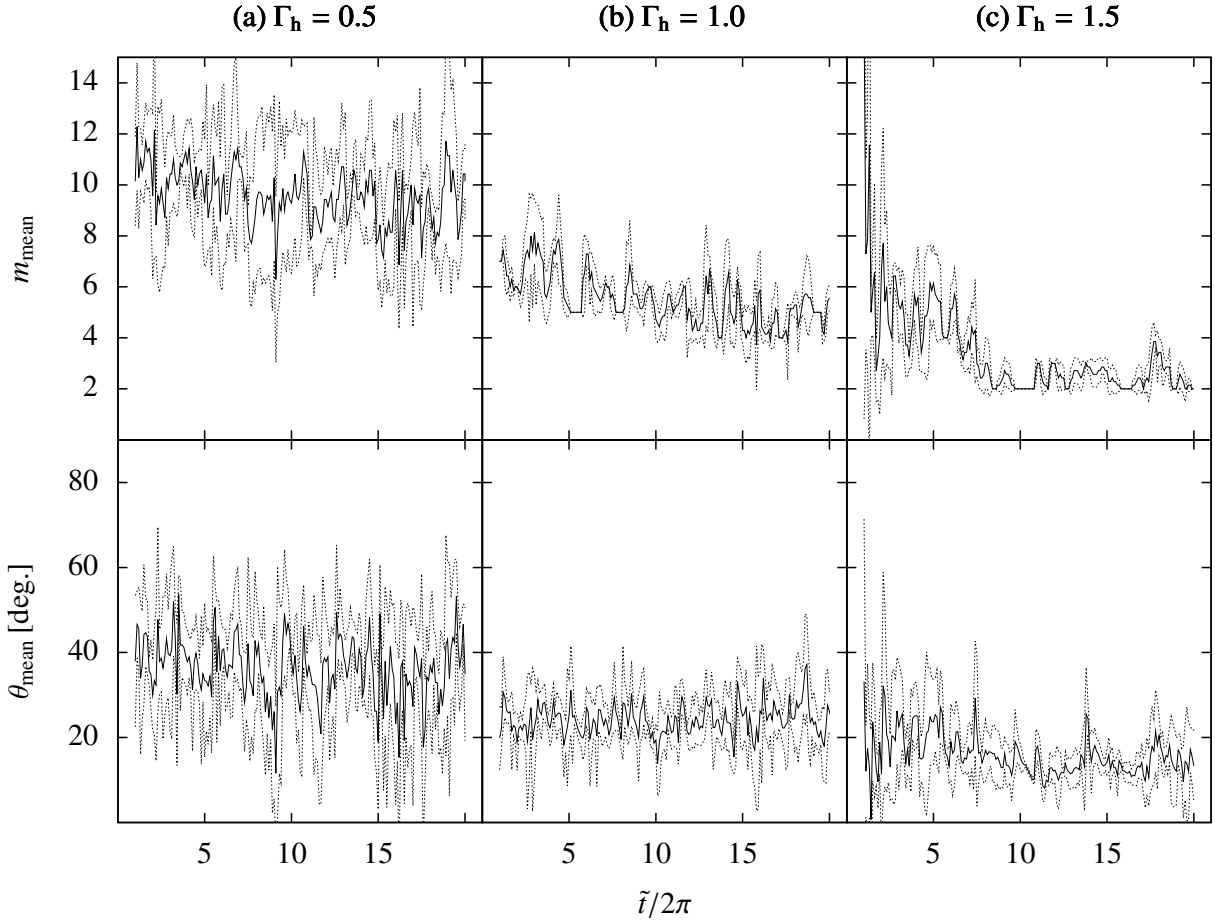


Figure 2. Time evolution of the averaged number of spiral arms $m_{\text{mean}}(\tilde{t})$ and the averaged pitch angle $\theta_{\text{mean}}(\tilde{t})$ for (a) $\Gamma_{\text{h}} = 0.5$ (model 2), (b) $\Gamma_{\text{h}} = 1.0$ (model 7), and (c) $\Gamma_{\text{h}} = 1.5$ (model 12). The solid curves represent $m_{\text{mean}}(\tilde{t})$ and $\theta_{\text{mean}}(\tilde{t})$. The dotted curves represent the quartile deviation.

The spiral arms are transient and recurrent, that is, the spiral arms are formed and destructed continuously. We find that the overall spiral arm structures, such as the pitch angle and the number, barely change with time for $\tilde{t}/2\pi > 10$.

For small Γ_{h} , the length scale of the spiral arms is short and their number is large, while for large Γ_{h} , the length scale is long and their number is small. Namely, the number of spiral arms decreases with increasing Γ_{h} . For larger Γ_{h} , the spiral arms are wound more tightly, in other words, the pitch angle is smaller.

Fig. 5 shows the evolution of Q for $Q_{\text{ini}} = 1.0, 1.2, 1.4, 1.6,$ and 1.8 (models 33, 35, 37, 39, 41). In a way similar to the calculation of $\bar{\theta}$ and \bar{m} , we calculate the average of Q . For smaller Q , Q increases more rapidly. This is consistent with the previous N -body simulations (Fujii et al. 2011, Paper I). In the case of smaller Q , the amplification factor is larger and the spiral arms are denser (Toomre 1981). Since the stars are scattered by the denser spiral arms more strongly, Q increases more rapidly. The time-averaged Q over $\tilde{t}/2\pi = 10$ –20 for each model is summarized in Table 1.

3.2 Comparison with Swing Amplification Theory

We examine the dependencies of $\bar{\theta}$ and \bar{m} on Γ , f , and Q . In Papers I and II, based on the swing amplification, \bar{m} and $\bar{\theta}$

are estimated as

$$\bar{m} = 0.922C \frac{(2 - \Gamma)^2}{fQ}, \quad (13)$$

$$\tan \bar{\theta} = \frac{1}{2\pi} \left(1 + \frac{2.095}{Q^{5.3}} \right)^{-1} \frac{\kappa}{A}, \quad (14)$$

where A is the Oort constant. In deriving equation (13) we assumed that the orbital frequency is given by $\Omega^2 \simeq \pi C G \Sigma_{\text{d}} / f r$ with a fudge factor C of order unity. Note that in reality C depends on the disk and halo models (see Appendix A). For the range of $Q = 1.5$ –1.8, equation (14) is reduced to

$$\tan \bar{\theta} \simeq \frac{1}{7} \frac{\kappa}{A} = \frac{2}{7} \frac{\sqrt{4 - 2\Gamma}}{\Gamma}. \quad (15)$$

3.2.1 Dependence on Γ

Fig. 6 shows the results of the N -body simulations. From Table 1, we adopt $Q \simeq 1.5$ for equations (13).

The number of spiral arms \bar{m} decreases with increasing Γ , which is consistent with equation (13). We find that equation (13) with $C = 1.5$ agrees well with the numerical results.

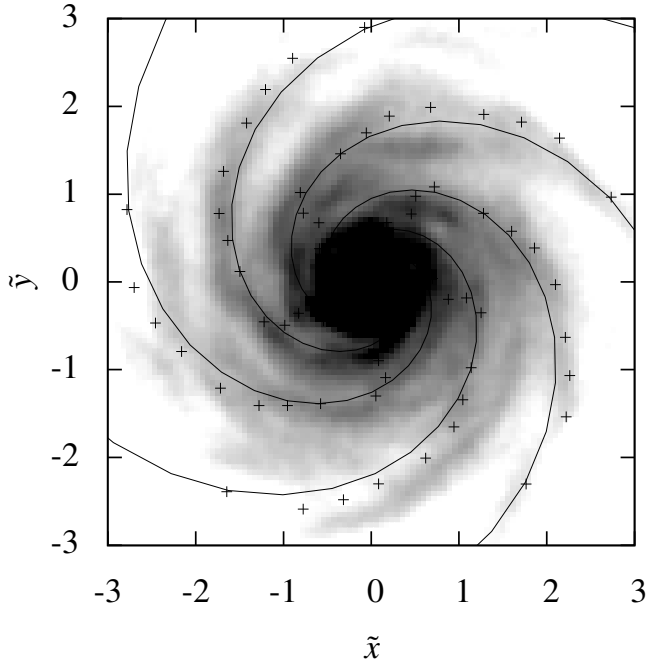


Figure 3. The density snapshot and the estimated spiral arms for $\Gamma_h = 1.0$, $f = 0.2$, and $Q_{ini} = 1.2$ (model 7) at $\tilde{t}/2\pi = 15.0$. The plus points denote the position of spiral arm estimated from the shape function ϕ_m with $m = 5$. The solid curves show the logarithmic spirals with $m = 5$ and $\theta = 24^\circ$.

The pitch angle $\bar{\theta}$ also decreases with increasing Γ . We find that equation (15) agrees well with the numerical results.

Fujii et al. (2018) performed the N -body simulations with a more realistic galactic model that includes a live bulge and dark matter halo. They compared the pitch angle with equation (15) and concluded that equation (15) agrees with the N -body simulations. Therefore, it is suggested that equation (15) is applicable under the general galactic models. In addition, they reported that a larger shear rate results in a smaller number of spirals. Our simulation results and equation (13) are also consistent with their results.

3.2.2 Dependence on f

Equation (13) with $C = 1.5$ shows that \bar{m} decreases with increasing f , which agrees with the N -body simulations. This result is consistent with the previous works (D’Onghia 2015; Fujii et al. 2018).

Equation (15) indicates that the pitch angle does not depend on f , which is confirmed by the N -body simulations. If we adopt $\Gamma = 1.0$ and $Q_{ini} = 1.2$, the mean pitch angle is 22° – 25° and is independent of f except for $f = 0.05$. In the case of the model with $f = 0.05$, the structure is too small and faint to calculate accurately the pitch angle.

Note that in the models adopted here, Γ and f are varied independently. Thus $\bar{\theta}$ is completely independent of f . Usually, a galaxy model with high f tends to have high Γ , where $\bar{\theta}$ depends on f through Γ .

3.2.3 Dependence on Q

Equations (13) and (15) show that \bar{m} decreases and $\bar{\theta}$ increases with increasing Q , but their dependencies are weak. The numerical results are consistent with the swing amplification.

3.2.4 θ – m Relation

We investigate the relation between the pitch angle and the number of spiral arms. The swing amplification mechanism gives its relation as (Paper II)

$$\bar{m} \simeq \frac{0.230C}{Qf} \left(\frac{14 \tan \bar{\theta}}{1 + \sqrt{1 + 49 \tan^2 \bar{\theta}}} \right)^4. \quad (16)$$

For $\bar{\theta} > 30^\circ$, this can be approximated by

$$\bar{m} \simeq 6.1C \left(\frac{\bar{\theta}}{40^\circ} \right) \left(\frac{f}{0.2} \right)^{-1} \left(\frac{Q}{1.5} \right)^{-1}. \quad (17)$$

Fig. 7 shows the results of N -body simulations with $f = 0.2$ (models 1–12), $f = 0.4$ (models 13–24) and $\Gamma_h = 1.0$ (models 25–32). In equations (16) and (17), we adopt $Q = 1.5$ and $C = 1.5$. The swing amplification mechanism generally agrees with the N -body simulations. Thus we predict that the pitch angle increases with the number of spiral arms if the spiral arms are formed by the swing amplification mechanism.

From the observational data, the positive correlation between the pitch angle and the number of spiral arms of unbarred multi-arm spiral galaxies has been reported (Hart et al. 2017). This correlation is consistent with equation (16). In order to confirm this relation in the observational studies more quantitatively, it is necessary to analyze θ – m relation together with f –dependence.

4 DISCUSSION

We present the intuitive derivation of the pitch angle and number of spiral arms. Except for the numerical coefficient, the pitch angle formula can be obtained from the phase synchronization argument (Michikoshi & Kokubo 2016b). We briefly summarize its derivation. We consider a single leading wave in a rotating frame. Due to the shear, the wave rotates from leading to trailing. When the wave changes from leading to trailing, the stabilizing effect of Coriolis force is reduced. Thus, the particles are pulled towards the wave center by the self-gravity and their epicycle phases are synchronized. Then the wave amplitude becomes the maximum after the half of an epicycle period (Michikoshi & Kokubo 2014). The pitch angle evolves with time as $\tan \theta = 1/(2At)$ where t is the elapsed time from $\theta = 90^\circ$. Substituting $t = \pi/\kappa$ we obtain the pitch angle as $\tan \theta \simeq \kappa/2\pi A$. This result is consistent with that of the local simulations and the swing amplification $\tan \theta \simeq \kappa/7A$ (Michikoshi & Kokubo 2014).

The azimuthal wavelength λ_y is given by the pitch angle θ and the radial wavelength λ_x ,

$$\lambda_y = \frac{\lambda_x}{\tan \theta}. \quad (18)$$

The radial wavelength is often assumed to be $\lambda_x = \lambda_{cr}$, where λ_{cr} is the critical wavelength of the gravitational instability for the axisymmetric modes (Toomre 1964). Though this

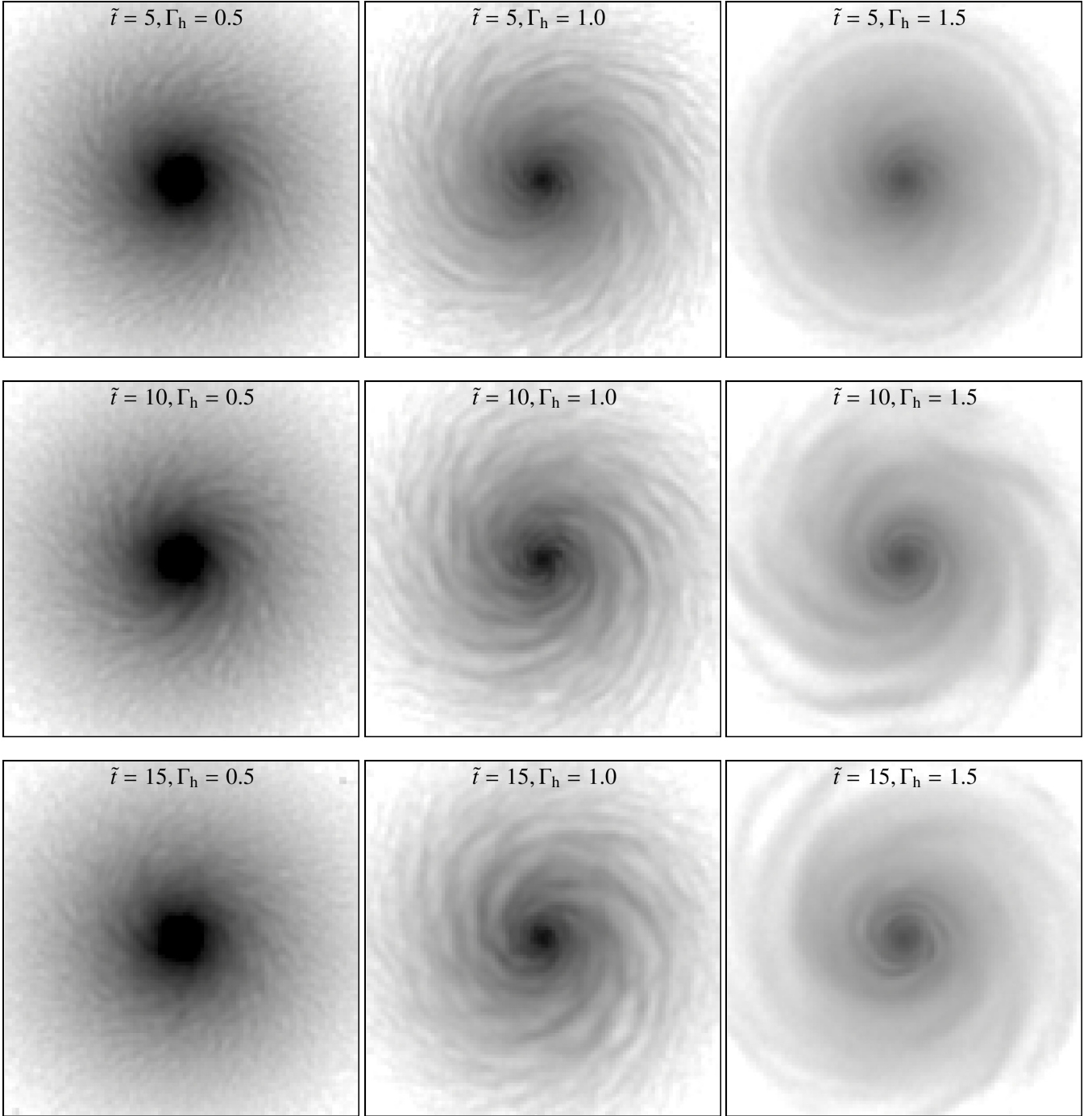


Figure 4. Snapshots of the surface density for $\Gamma_h = 0.5$ (model 2), 1.5 (model 7), and 1.5 (model 12) at $\tilde{t}/2\pi = 5.0, 10.0$ and 15.0. The surface density is shown in logarithmic scale in the region of $-5 \leq \tilde{x} \leq 5$ and $-5 \leq \tilde{y} \leq 5$.

relation is not obvious for non-axisymmetric modes, the local linear analyses of the swing amplification and the local N -body simulations confirm $\lambda_x \simeq \lambda_{cr}$ for $\kappa/\Omega < 1.6$ (Michikoshi & Kokubo 2016a). Thus, adopting this relation we obtain

$$\lambda_y = \frac{\lambda_{cr}}{\tan \theta} \simeq \frac{28\pi^2 G \Sigma_d A}{\kappa^3}. \quad (19)$$

Using the azimuthal wavelength, we calculate the number of

spiral arms as

$$m = \frac{2\pi r}{\lambda_y} \simeq \frac{\kappa^3 r}{14\pi G \Sigma_d A} \sim \frac{\kappa^3}{14 f A \Omega^2}, \quad (20)$$

where we used the approximation $\Omega^2 \simeq \pi G \Sigma_d / r f$ (Paper II, Appendix A). For $1.0 < \kappa/\Omega < 1.5$, we numerically find that $A\kappa/\Omega^2$ is almost constant between 0.65 and 0.77. Thus in this parameter range, we can approximate $A\kappa/\Omega^2$ as a constant 0.71. This approximation can recover the previous result,

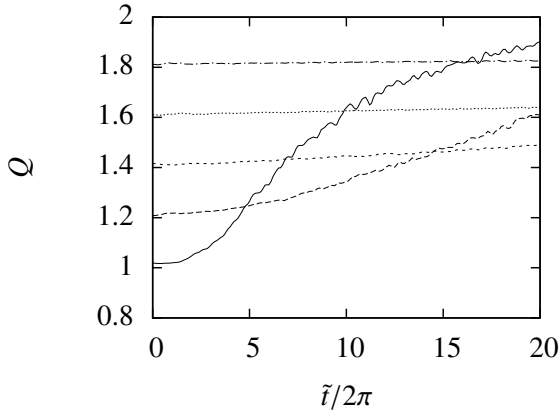


Figure 5. Time evolution of Q for $Q_{\text{ini}} = 1.0, 1.2, 1.4, 1.6,$ and 1.8 (models 33, 35, 37, 39, 41).

which is

$$m \sim 0.1 \frac{\kappa^4}{f\Omega^4}. \quad (21)$$

This expression agrees with that obtained by the swing amplification (equation (13)) except for the dependence on Q .

In the above argument we assumed that $\lambda_x \simeq \lambda_{\text{cr}}$. On the other hand, λ_y increases with Γ and decreases with increasing θ since θ decreases with increasing Γ . This indicates that m is larger for larger θ , which is consistent with equation (16).

5 SUMMARY

We have performed the global N -body simulations of disk galaxies in order to compare the spiral structure with those by the swing amplification theory. The mean pitch angle and number of spiral arms were calculated in the disks with various shear rates and mass fractions. We confirmed that the dependencies of the spiral structure on disk parameters agree with those in the swing amplification theory. The pitch angle decreases with increasing the shear rate and is independent of the disk mass fraction. The number of spiral arms decreases with both increasing the shear rate and the disk mass fraction. It follows that the pitch angle tends to increase with the number of spiral arms if the disk mass fraction is fixed.

From the swing amplification mechanism only we cannot understand the overall process of the spiral arm formation. The N -body simulations show that the spiral arms are transient and recurrent, that is, the spiral arms are formed and destructed continuously. Two questions remain unsolved in this process. One is the origin of seed leading waves. In the realistic galaxies, the swing amplification mechanism requires relatively strong leading waves. The N -body simulations show that the overdense or underdense regions forms due to the nonlinear interaction between spiral arms (D’Onghia et al. 2013; Kumamoto & Noguchi 2016). However, its physical mechanism is still unclear. We have to understand the generation mechanism such leading waves.

The other is the fate of the amplified spiral arms. The N -body simulations show that the amplified arms are finally destructed. The destruction mechanism has not yet been understood completely. Baba et al. (2013) pointed out that the stars in spiral arms escape and the spiral arms damp due to the non-linear wave-particle interaction. It is also suggested that the nonlinear wave-wave interaction generates the leading arms from the swing-amplified arms (Fuchs et al. 2005). The wave-wave interaction may also contribute to damping of the spiral arms. In addition, the gas component of the disk neglected in the present study, may potentially affect the dynamics of spiral arms (e.g., Bottema 2003). Further study on this effect is necessary.

In our N -body simulations, we adopt a artificial galactic model and generate the initial condition by simple manner to control the key disk parameters. Our results suggest that a fudge factor in equation (13) depends on the galactic model. Thus, it is necessary to determine this factor for more realistic galactic model. In addition, the initial condition of our model is not exactly in an equilibrium. Thus, we adopt the randomizing-azimuthal method for avoiding unnatural structures (McMillan & Dehnen 2007; Fujii et al. 2011). It would be better to adopt the more sophisticated method for generating initial conditions (Hernquist 1993; Kuijken & Dubinski 1995; McMillan & Dehnen 2007; Miki & Umemura 2018). In the future work, we will validate the swing amplification theory base on more realistic model.

Numerical computations were carried out on Cray XC30 at Center for Computational Astrophysics, National Astronomical Observatory of Japan.

ACKNOWLEDGEMENTS

Numerical computations were carried out on ATERUI (Cray XC30) at the Center for Computational Astrophysics, National Astronomical Observatory of Japan.

REFERENCES

- Athanassoula E., 1984, *Phys. Rep.*, **114**, 319
 Baba J., 2015, *MNRAS*, **454**, 2954
 Baba J., Asaki Y., Makino J., Miyoshi M., Saitoh T. R., Wada K., 2009, *ApJ*, **706**, 471
 Baba J., Saitoh T. R., Wada K., 2013, *ApJ*, **763**, 46
 Binney J., Tremaine S., 2008,
 Bottema R., 2003, *MNRAS*, **344**, 358
 Buta R., Vasylyev S., Salo H., Laurikainen E., 2005, *AJ*, **130**, 506
 Carlberg R. G., Freedman W. L., 1985, *ApJ*, **298**, 486
 D’Onghia E., 2015, *ApJ*, **808**, L8
 D’Onghia E., Vogelsberger M., Hernquist L., 2013, *ApJ*, **766**, 34
 Dobbs C. L., Theis C., Pringle J. E., Bate M. R., 2010, *MNRAS*, **403**, 625
 Freeman K. C., 1970, *ApJ*, **160**, 811
 Fuchs B., Dettbarn C., Tsuchiya T., 2005, *A&A*, **444**, 1
 Fujii M. S., Baba J., Saitoh T. R., Makino J., Kokubo E., Wada K., 2011, *ApJ*, **730**, 109
 Fujii M. S., Bédorf J., Baba J., Portegies Zwart S., 2018, *MNRAS*, **477**, 1451
 Goldreich P., Lynden-Bell D., 1965, *MNRAS*, **130**, 125
 Grand R. J. J., Kawata D., Cropper M., 2013, *A&A*, **553**, A77
 Hart R. E., et al., 2017, *MNRAS*, **472**, 2263
 Hernquist L., 1990, *ApJ*, **356**, 359

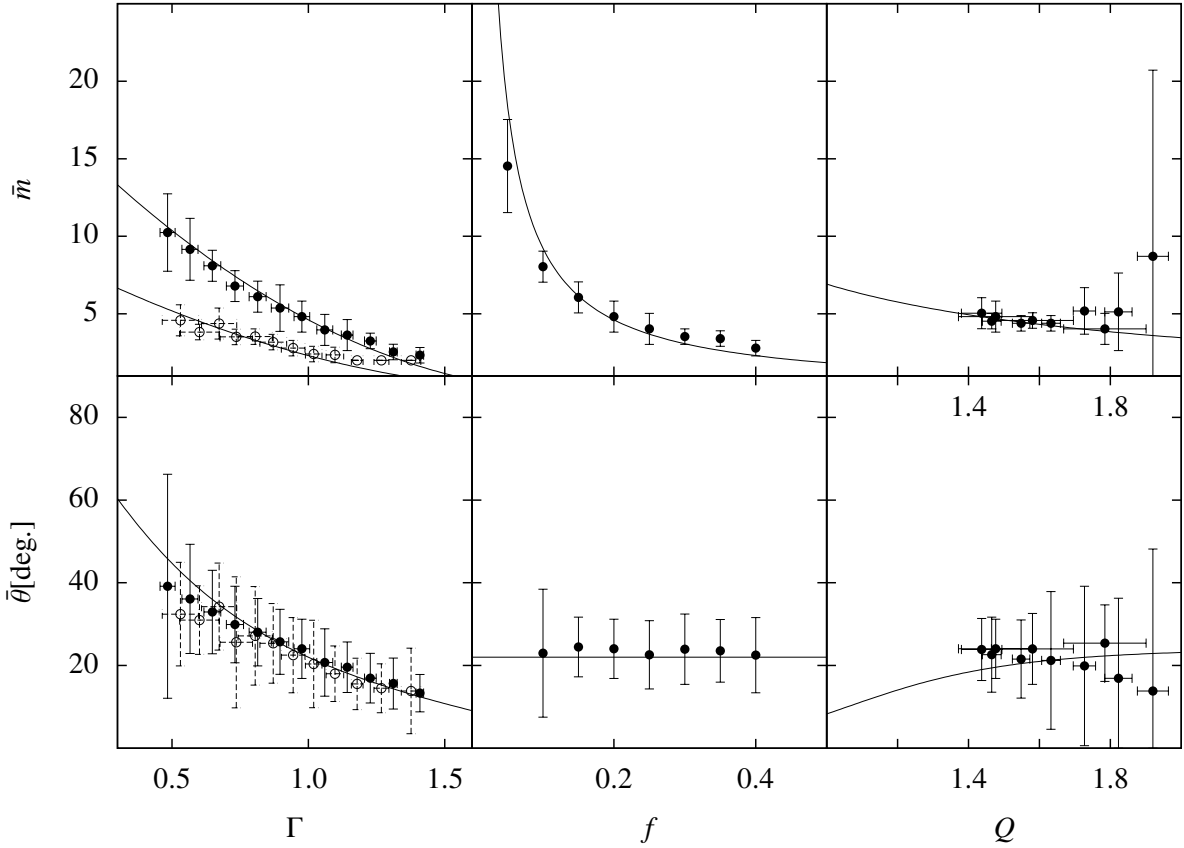


Figure 6. Number of spiral arms \bar{m} and the pitch angle and $\bar{\theta}$ against Γ , f , and Q . In the top panels (number of spiral arms \bar{m}), the solid curves show equation (13) with $C = 1.5$. In the bottom panels (pitch angle θ), the solid curves show equation (15). In the left panels (Γ -dependence), the filled and open circles correspond to the models of $f = 0.2$ (models 1–12) and $f = 0.4$ (models 25–32), respectively. The error bars represent quartile deviation.

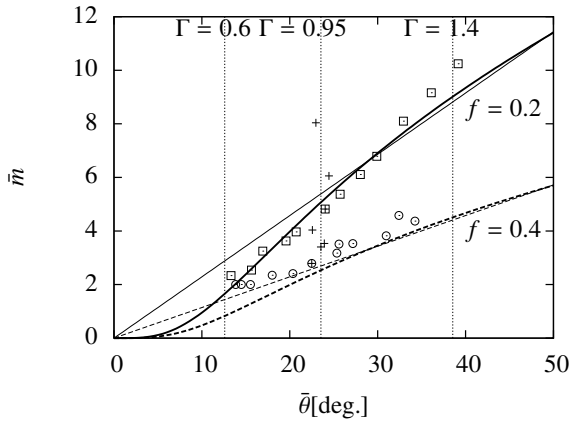


Figure 7. Pitch angle $\bar{\theta}$ against the number of the spiral arms \bar{m} for the models of $f = 0.2$ (models 1–12, squares), $f = 0.4$ (models 13–24, circles), and $\Gamma_h = 1.0$ (models 25–32, pluses). The solid and dashed thick curves show the estimates given by equation (16) with $f = 0.2$ and $f = 0.4$, respectively. The factor $C = 1.5$ and $Q = 1.5$ are adopted. The thin lines show the approximated estimate given by equation (17). The vertical dotted lines show equation (15) with $\Gamma = 0.6, 0.95$, and 1.4 .

- Hernquist L., 1993, *ApJS*, **86**, 389
 Ida S., Kokubo E., Makino J., 1993, *MNRAS*, **263**, 875
 Iwasawa M., Tanikawa A., Hosono N., Nitadori K., Muranushi T., Makino J., 2016, *PASJ*, **68**, 54
 Julian W. H., Toomre A., 1966, *ApJ*, **146**, 810
 Kuijken K., Dubinski J., 1995, *MNRAS*, **277**, 1341
 Kumamoto J., Noguchi M., 2016, *ApJ*, **822**, 110
 Lewis J. R., Freeman K. C., 1989, *AJ*, **97**, 139
 McMillan P. J., Dehnen W., 2007, *MNRAS*, **378**, 541
 Michikoshi S., Kokubo E., 2014, *ApJ*, **787**, 174
 Michikoshi S., Kokubo E., 2016a, *ApJ*, **821**, 35
 Michikoshi S., Kokubo E., 2016b, *ApJ*, **823**, 121
 Michikoshi S., Kokubo E., 2017, *ApJ*, **837**, L13
 Michikoshi S., Fujii A., Kokubo E., Salo H., 2015, *ApJ*, **812**, 151
 Miki Y., Umemura M., 2018, *MNRAS*, **475**, 2269
 Navarro J. F., Frenk C. S., White S. D. M., 1997, *ApJ*, **490**, 493
 Oh S. H., Kim W.-T., Lee H. M., Kim J., 2008, *ApJ*, **683**, 94
 Salo H., 1995, *Icarus*, **117**, 287
 Seigar M. S., Block D. L., Puerari I., Chorney N. E., James P. A., 2005, *MNRAS*, **359**, 1065
 Sellwood J. A., 2000, *Ap&SS*, **272**, 31
 Sellwood J. A., Carlberg R. G., 1984, *ApJ*, **282**, 61
 Tanikawa A., Yoshikawa K., Okamoto T., Nitadori K., 2012, *New Astron.*, **17**, 82
 Tanikawa A., Yoshikawa K., Nitadori K., Okamoto T., 2013, *New Astron.*, **19**, 74
 Toomre A., 1964, *ApJ*, **139**, 1217
 Toomre A., 1981, *pp 111–136*

APPENDIX A: ESTIMATION OF FACTOR C

We describe the approximation that we employed in deriving the number of spiral arms in Paper II. Considering the azimuthal wavelength λ_y , the number of spiral arms is written as

$$m = \frac{2\pi r}{\lambda_y} = \frac{1}{2.17 \cdot 2\pi Q} \frac{r\Omega^2}{G\Sigma_d} \left(\frac{\kappa}{\Omega}\right)^4, \quad (\text{A1})$$

where we used $\lambda_y = 2.17Q(\Omega/\kappa)^2\lambda_{\text{cr}}$ (Paper II). We assume that the orbital frequency is

$$\Omega^2 \simeq \frac{GM_{\text{tot}}}{r^3}, \quad (\text{A2})$$

where M_{tot} is the total mass inside the sphere with radius r . In addition, we assume that the disk mass inside the sphere with radius r is roughly given by $\pi r^2 \Sigma_d$. Thus, M_{tot} is given as

$$M_{\text{tot}} \simeq \frac{\pi r^2 \Sigma_d}{f}. \quad (\text{A3})$$

Substituting equation (A3) into equation (A2), we obtain

$$\Omega^2 = \frac{\pi C G \Sigma_d}{f r}, \quad (\text{A4})$$

where we introduce a fudge factor C . Substituting equation (A4) into equation (A1), we obtain the number of spiral arms with a factor C (equation (13)). We expect that C is an order of unity, though its value depends on the disk and halo models. In what follows, we estimate C assuming an exponential disk and a power-law halo models.

The orbital frequency is separated into two components,

$$\Omega^2 = \Omega_{\text{h}}^2 + \Omega_{\text{d}}^2, \quad (\text{A5})$$

where Ω_{d} is the contribution by the disk given by

$$\Omega_{\text{d}}^2 = \frac{\pi G \Sigma_{\text{d0}}}{r_0} (I_0(\tilde{r}/2)K_0(\tilde{r}/2) - I_1(\tilde{r}/2)K_1(\tilde{r}/2)), \quad (\text{A6})$$

where I_ν and K_ν are the modified Bessel functions of the first and second kinds and ν is an order (Freeman 1970). Substituting equations (2) and (A6) into equation (A5), we obtain

$$C = \frac{f r \Omega^2}{\pi G \Sigma_d} = \frac{e^{\tilde{r}}}{2} \left(1 - \frac{3}{e^2}\right) \left(\frac{\tilde{r}}{2}\right)^{1-2\Gamma_{\text{h}}} (1 + C_f f), \quad (\text{A7})$$

where

$$C_f = \frac{4(I_0(\tilde{r}/2)K_0(\tilde{r}/2) - I_1(\tilde{r}/2)K_1(\tilde{r}/2))}{1 - 3/e^2} \left(\frac{\tilde{r}}{2}\right)^{2\Gamma_{\text{h}}} - 1. \quad (\text{A8})$$

As shown in Fig. A1, C_f depends on Γ_{h} and \tilde{r} , which ranges from -0.5 to 0.8 . The averaged value over $1 < \tilde{r} < 2$ and $0.5 < \Gamma_{\text{h}} < 1.5$ is about 0.20 . Thus, if f is not large, we can use the approximation $C_f f \simeq 0$. The factor C with $C_f f \simeq 0$ is shown in Fig. A1. We obtain that C averaged over for $1 < \tilde{r} < 2$ and $0.5 < \Gamma_{\text{h}} < 1.5$ is 1.85 . Therefore, $C \simeq 1.85$ is a good approximation.

This paper has been typeset from a $\text{\TeX}/\text{\LaTeX}$ file prepared by the author.

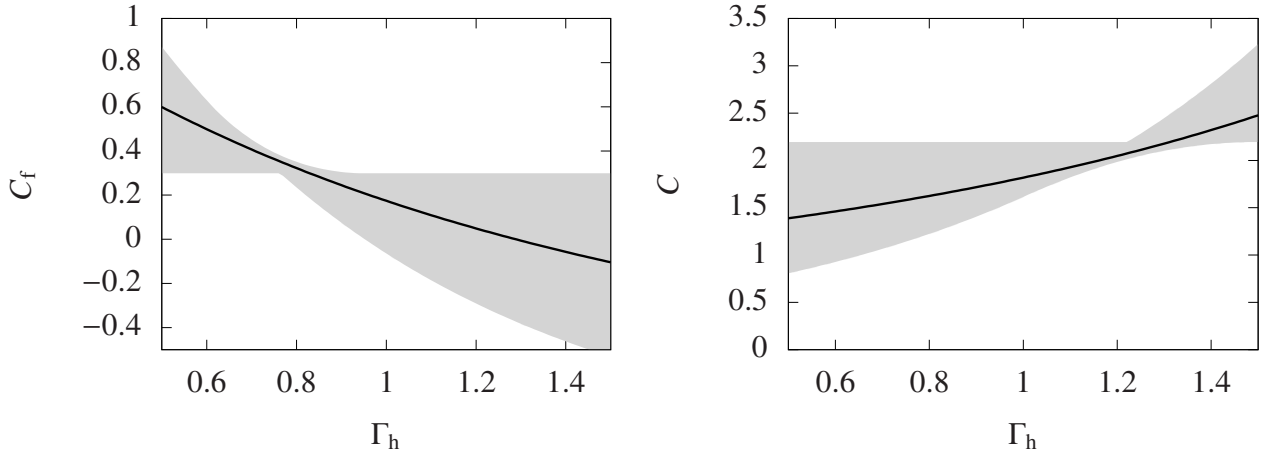


Figure A1. Factors C_f and C as a function of Γ_h . The solid curves show the values averaged over $\tilde{r} = 1-2$. The shaded regions show the minimum and maximum values for $\tilde{r} = 1-2$. In calculating C , we assumed $C_{ff} = 0$.